A Roughness, Feature-based Algorithm of Point Cloud Segmentation of the Secondary Lining in NATM Tunnel

Tiantao Zhang, Lizhuang Cui, Lizhi Zhou, Jian Liu, Lei Kou* and Quanyi Xie*

School of QiLu Transportation, Shandong University, 250061 Jinan, China
TTZHANG@sdu.edu.cn, lizhuang.cv@mail.sdu.edu.cn,
202320878@mail.sdu.edu.cn, lj75@sdu.edu.cn, lei.kou@sdu.eud.cn,
xiequanyi@sdu.edu.cn

Abstract: To realize point cloud segmentation of secondary lining in tunnel under construction, a roughness feature-based point cloud segmentation algorithm for secondary lining is developed in this paper. Preprocessing of raw scanned data enables the parameterization of the optimal voxel mesh size, roughness calculation radius and extraction threshold with algorithm experiments. Primary segmentation is performed by clustering under optimal parameters, and then the results of the primary segmentation are input as seed points for secondary segmentation. The effective segmentation rate is up to 99.25%. Comparison confirms that the performance of the proposed algorithm is superior to other similar algorithms, proving its' practicality and feasibility.

Keywords: Tunnel; Point Cloud; Secondary Lining; Segmentation Algorithm

1 Introduction

The economic development experience of various countries around the world has attested to the necessity of a fast and smooth transportation network [1-3]. As the economy develops, a large number of countries have developed tunnel engineering, whose construction management has received extensive attention from specialists and scholars [4-6]. The New Austrian Tunneling Method (NATM) proposed in the 1950s has been widely implemented in 70% to 80% of mountain tunnels in Europe after years of practice and promotion [7-9]. The secondary lining, as an indispensable component of the NATM tunnel, has also attracted a lot of attention [10-12].

With the continuous advancement of construction techniques and mechanization, the demand for intelligent tunnel construction is also increasing. Point clouds, as a three-dimensional (3D) visualization tool for describing the real-world

environments, have attracted great attention in computer vision field [13] [14]. The significant advantages of point clouds in terms of fast acquisition speed and accurate geometric representation have led to increasing utilization of 3D point clouds for a variety of tasks, including construction quality inspection and progress tracking [15] [16]. In addition, point clouds can provide detailed spatial information and point features for accurate and refined object reconstruction and segmentation [17]. First of all, point cloud data can provide high-precision three-dimensional spatial information. By fine segmentation of the point cloud data, the lining thickness can be determined more accurately, thus improving the lining quality. Second, the point cloud information can more accurately determine the shape and features inside the tunnel, thus improving the accuracy of positioning and sizing. Then, the quality of the lining can be assessed more accurately, such as the consistency of the lining thickness and the flatness of the tunnel interior, thus improving the quality of the project. Finally, through the fine segmentation of the point cloud data, hidden hazards inside the tunnel, such as cracks, corrosion, and exposure of steel reinforcement in the inner wall of the tunnel, can be more accurately identified, thus improving the safety of the project. Therefore, it is extremely crucial to segment the secondary lining of tunnels under construction through point cloud data, which provides the basis for intelligent detection of a series of problems that may arise during the construction of secondary lining.

Various inter-enclosed support objects in complex tunnel environments, such as trolleys, pipelines and so on, generally generate a large number of interfering point clouds that interfere with the segmentation of the secondary lining. Some reported denoising methods are positive for removing the obvious noise and outliers [18] [19], but it is still difficult to minimize the influence of ancillary structures in tunnel on segmentation. For tunnel lining segmentation, least square method or Ransac [20] [21] can be applied to obtain the tunnel profile by fitting cylinders [22] [23]. This is only applicable to shield tunnels with regular cross-sectional profiles, whereas the profiles of highway tunnels are in three-centered circles. The actual situation is not exactly the same as the design drawings, making it difficult to determine the formulas and parameters to be used for fitting. The region growth algorithm [24] can also be employed for region segmentation of the tunnels [25]. However, the curvature, which is a key factor affecting the region growth, does not effectively distinguish between initial support and secondary support. A large number of point cloud deep learning methods [26-28] have been proven to be highly effective for classification and segmentation tasks of the point clouds, but they still suffer from the problems of limited measurement data and unknown actual segmentation results when dealing with larger outdoor objects such as the tunnels under construction. Currently, most of the segmentation tasks for tunnels are concentrated in segment linings, lines, contact networks and so on in subway tunnels [29-31]. In these studies, the segmented tunnel environments were more regular and well-organized than the tunnels under construction, and the point cloud is mainly the structural part of the tunnel without a large number of interference point clouds.

This paper proposes a roughness, feature-based segmentation algorithm, for secondary lining point clouds of the tunnels under construction. The raw scanned data are preprocessed, where the optimal voxel mesh size, roughness calculation radius and extraction threshold are determined by algorithm experiments. Primary segmentation is performed by clustering under optimal parameters, and then the results of the primary segmentation are input as seed points for secondary segmentation. The developed algorithm is evaluated and compared with similar algorithms, and it is confirmed that the algorithm reduce computational complexity as well as provide good applicability and segmentation integrity for complex tunnel scenarios.

2 Data Acquisition and Preprocessing

In view of the large amount of the point cloud scenario data obtained through mobile scanning and complex tunnel environments, a roughness feature-based fast segmentation algorithm for secondary lining point clouds is proposed. The specific implementation scheme is described as follows, obvious outliers and noise points in the point cloud data are removed with software. During the analysis process, the points such as silhouettes, vehicles, etc. that appear during the scanning process are considered as noisy points that have nothing to do with the structure. After the point cloud data is solved, there are some points outside the tunnel which are considered as outliers.

2.1 Acquisition of Experimental Data

The laser 3D scanning technique is applied to acquire point cloud data in a highway tunnel under construction in Shandong Province, China. For point cloud data acquisition, a Hovermap mobile 3D laser scanner is used for tunnel scanning, and the main procedures involve scanning route setting, point cloud data collection, on-site data inspection, data export and backup. The maximum scanning distance of the scanner is 100 m, with a distance measurement accuracy of ±5 mm and a measurement range of 360°.

A typical tunnel scenario with complex structures and machinery is selected from the scanned tunnel point cloud data to for investigation of the applicability of the algorithm. The scenario includes various lining situations at different periods, such as the initial support with steel mesh, the initial support blocked by the trolley, the initial support and the secondary lining, as well as various machinery such as the trolley, vehicles and construction equipment. When evaluating the algorithm, it is necessary to know the number of points in the original secondary lining in Fig. 1. In view of this, Cloud Compare software is used to manually segment each structure and calculate the number of points in the secondary lining, initial support and other parts as the evaluation indicators for subsequent algorithms.

The total number of point cloud data after preprocessing the raw data is 1,834,237, where the numbers of points in the initial support, secondary lining, mechanical vehicle and road surface are 814,299, 394,605, 126,020 and 499,313, respectively.

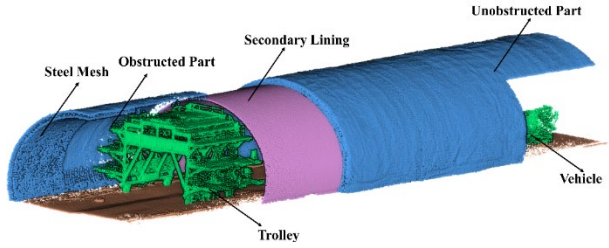

Figure 1
Composition of Point Cloud Data

2.2 Data Preprocessing

The purpose of data preprocessing is to remove shadow points and noise generated by the movement of vehicles and personnel during mobile scanning, and to improve the accuracy and availability of point cloud data in feature extraction. 3D point clouds are usually characterized by complex, multidimensional, and large-scale features, while the additional data unrelated to original objects are easily generated during the acquisition process due to the complex environment. Therefore, special processing of point clouds, such as data cleaning, is crucial for effective acquisition and accurate analysis. The data cleaning of the point clouds typically involves filtering and removal of unnecessary, occluded or erroneous points. The next step after removing the noise is to clarify the point cloud information in the point cloud data that is not related to the tunnel structure, such as the steel frame structure, construction vehicles, and construction workers, as shown in Figure 2.

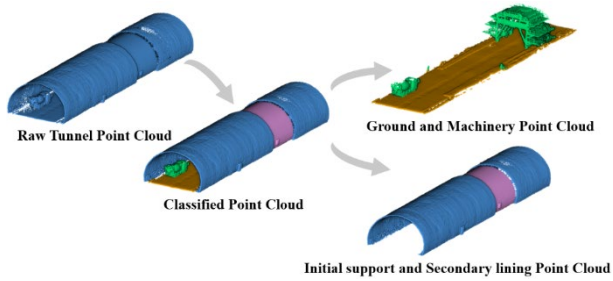

Figure 2
Data preprocessing manual filtering

In this paper, some points that appear during scanning are considered that don't matter to the structure such as silhouettes, vehicles, etc. as noise points. Then after the point cloud is solved there are some points on the outside of the tunnel, which are considered as outliers, as shown in Figure 3.

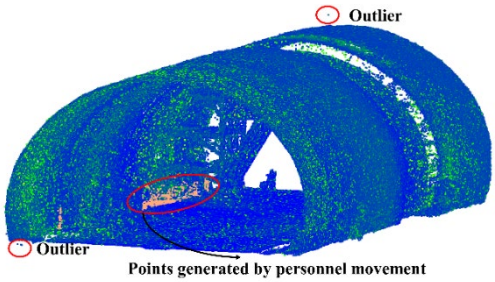

Figure 3
Data preprocessing of Outlier

3 Algorithm

3.1 Algorithm Feasibility Analysis

The normal vectors of the point clouds of the initial support and secondary lining are calculated, and they are then rendered based on the normal vector values. The normal vectors along the X, Y, and Z coordinate axes of the point clouds of the initial support and the secondary lining are analyzed to determine their differences in roughness.

Figure 4 presents the normal vectors of the point cloud data in the X, Y and Z directions. It can be seen that the normal vectors of the initial support and secondary lining differ in different directions. Figure 5 illustrates the tunnel orientation roughly along the X-axis, where the normal vector values of the initial support and secondary lining are concentrated between -0.15 and 0.15 while those of the initial support are mainly concentrated between -0.4 and 0.3. As the tunnel direction is mainly along the X-axis, the components of the point cloud data on the X-axis are smaller. However, due to the unevenness of the secondary lining surface, its Nx is larger with a wider distribution. The normal vectors of the point clouds along the Y-axis direction in the initial support change uniformly along the circumference of the tunnel; however, the normal vectors of the secondary lining on tunnel sidewalls change abruptly. Therefore, a peak in the range of 0.8 to 1.0 appears in figure (c), whereas no such change appears in figure (d). This also indicates that the Ny mainly characterizes the changes on the tunnel sidewalls, and the initial support causes an abrupt change in Ny as a result of the concavity. The same situation exists for the normal vectors in the Z-axis direction, where the secondary lining varies uniformly along the circumference of the tunnel and the initial support varies abruptly at the top of the tunnel. Namely, there is a peak on the right side of figure (e), while there is no such peak in figure (f). The above analysis determines that there is a roughness difference between the secondary lining and the initial support in point cloud data.

This difference can be shown by the normal vectors, determining the feasibility of the subsequent algorithms.

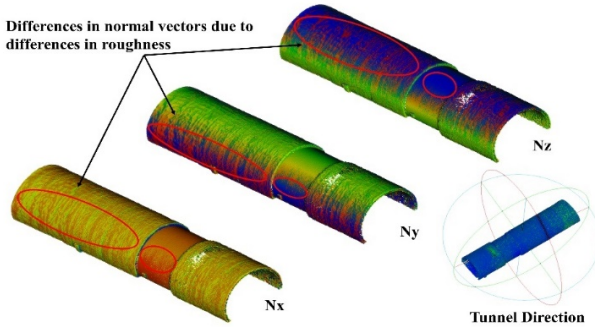

Figure 4
Tunnel point clouds under three normal vector components

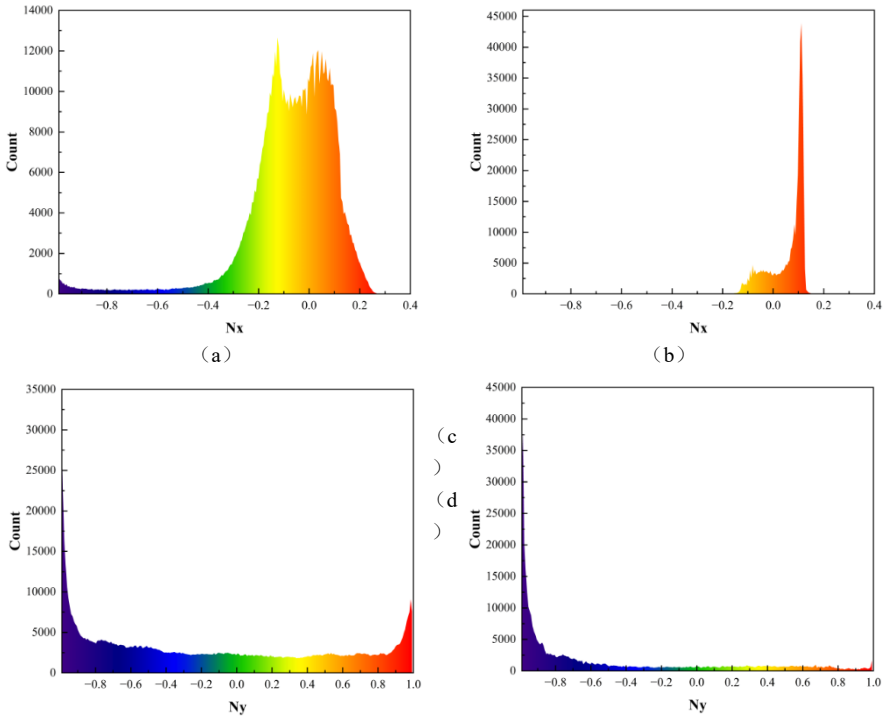

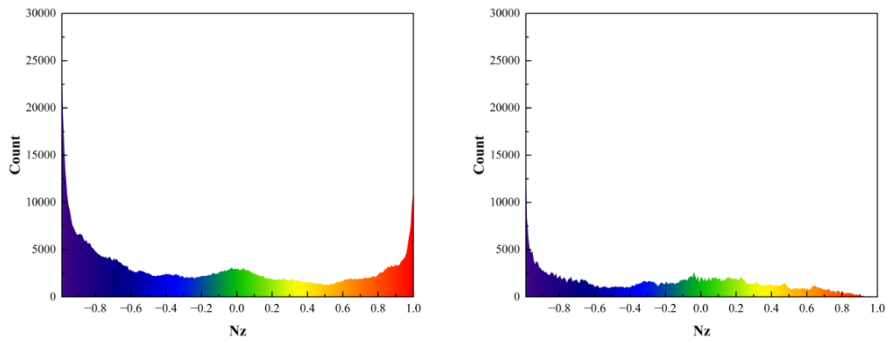

Figure 5

The normal vector components of the point clouds in initial support and secondary lining: (a) initial support Nx, (b) secondary lining Nx, (c) initial support Ny, (d) secondary lining Ny, (e) initial support Nz, (f) secondary lining Nz

3.2 Downsampling and Initial Segmentation

3D point clouds often contain a large amount of redundant data, which requires a lot of computation and takes a long time to process directly. Therefore, it is necessary to downsample them. Downsampling is also a key step in the point cloud preprocessing. This study performs downsampling with a voxel grid method and discretizes the computed bounding box of the point clouds into small voxels. The length, width, and height dimensions of voxels can be set parametrically, or the number of voxels in each of the three directions can be specified to obtain a set of points that fall within each voxel. One sampled point is taken from each voxel to replace the original point set. It is characterized by high efficiency, relatively uniform distribution of sampling points and controllable indirect spacing of sampling points.

In this study, the point intensity is reduced by downsampling to save the computational time. However, reducing the point intensity also leads to a partial loss of the point cloud data. To reduce the impact of missing point clouds on secondary segmentation, the optimal point intensity of the algorithm, i.e., the average distance between point clouds, is determined through algorithm experiments in the follow-up works. The point intensity of the point clouds can be indirectly controlled by dividing the voxel grid, which improves the processing efficiency while ensuring the accuracy of segmentation.

Roughness in present study is defined as: for each point, the value of ‘roughness’ was equal to the distance between the point and the best fit plane in a certain neighborhood. The best fit plane is determined with the least squares method. To obtain unknown parameters in the least squares method, 3D data of the plane are assumed, and the plane is defined as.

$$ax+by+cz+d=0 \tag{1}$$

where the a, b, c, and d are all the plane parameters.

For all point clouds, in formula (2) a Covariance matrix is constructed:

$$M_{3\times3}=\frac{1}{m}\sum_{i=1}^{m}(p_i-\bar{p})(p_i-\bar{p})^T \tag{2}$$

$$\bar{p}=\frac{1}{m}\sum_{i=1}^{m}p_i \tag{3}$$

where $p_i \in P$; $\bar{p}$ is the center point of all points in point set P.

The Eigenvalues and eigenvectors of covariance M are calculated according to formula $\lambda V=MV$, where $\lambda=(\lambda_0,\lambda_1,\lambda_2)$ is the eigenvalue of M and $V=(V_0,V_1,V_2)$ is eigenvectors corresponding to λ. The four parameters a, b, c and d are calculated by obtaining the minimum value of each eigenvalue to obtain the best fitting plane. And the distance from the point to the plane is calculated as a rough value in present study.

After downsampling, each point in the point clouds corresponds to a roughness value after roughness calculation as shown in Figure 6. The roughness values of the secondary lining are relatively small and uniform, while those of the initial support are relatively large and partially non-uniform. Point clouds with roughness values within a certain range are roughly extracted, where the most of the secondary lining point clouds are preserved and the remaining point clouds of the initial support, ground and trolley are fragmented. Considering these differences between the coherence and incoherence, fragmentation and uniformity, Euclidean clustering are used to segment secondary point clouds from all point clouds to achieve initial segmentation in the algorithm.

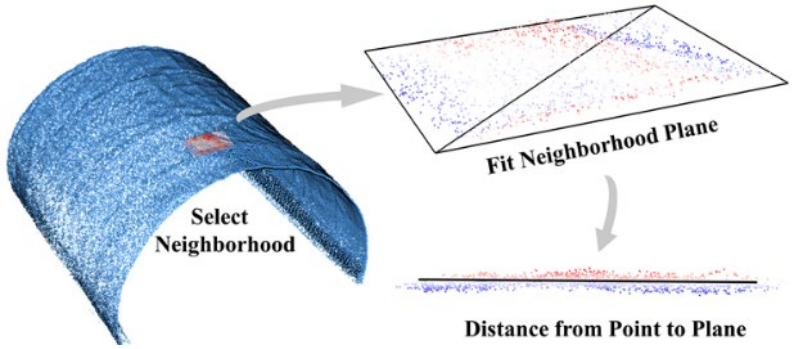

Figure 6
Schematic diagram of roughness principle

3.3 Secondary Segmentation

Generally, the segmentation task is to perform further processing of the initial results such as establishment of the model, acquisition of detailed parameters and other subsequent steps. For the smooth running of the subsequent tasks, it is very important to avoid data loss caused by segmentation as much as possible, so that more details in the raw data can be preserved. In the previous initial segmentation, the segmented objects are the downsampled point clouds, so the segmentation results obtained have a relatively small number of point clouds that lack many details and even show some holes. To obtain the secondary point clouds close to the raw scanning data, a secondary segmentation is conducted.

Available algorithms usually process up-sampling with rich point cloud intensity, but the up-sampling is often calculated and fitted by the relationship of surrounding points, which does not recover the varying scenarios very well. Also, the up-sampling is usually performed without the raw data. This study was inspired by the clustering algorithm that uses seed points to segment the required point clouds. The point clouds obtained from the first segmentation are used as the seed points for further segmentation by searching the surrounding points through the kd-tree. To attain as many secondary point clouds as possible, the search radius is usually set to exceed the distance between the seed points, which may lead to duplicate point acquisition. The results obtained from the second segmentation are filtered on one side, and the duplicate points are deleted, as shown in Figure 7

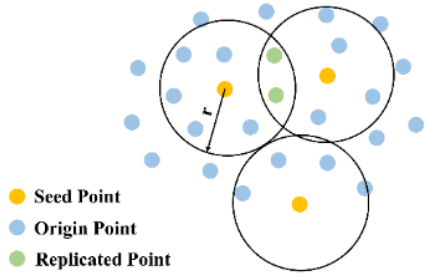

Figure 7
Schematic diagram of secondary segmentation

4 Experiment Result

4.1 Optimal Point Density

The work in this section is performed to improve computational efficiency. The complexity would be greatly increased if the point cloud data are not downsampled. Determining a reasonable downsampling parameter, i.e., the final

point density, is crucial because point intensity not only affects computational efficiency but also the subsequent segmentation. Therefore, the data should not be too dense or sparse. The present study changes the point intensity or average point spacing by setting the size of the voxel grid. The original point intensity is about 0.03 m, and the voxel grid is set between 0.04 -0.10 m, with an increase of 0.01 m each time. A total of 7 sets of experiments are conducted.

Table 1 illustrates the average point spacing, the number of filtered secondary points, the number of secondary points obtained in a single segmentation and the number of over-segmented points under 7 voxel grids. As the voxel grid increases, the number of points decreases, resulting in a decrease in the number of segmented points. The effectiveness of the segmentation cannot be confirmed by the number of points alone. Therefore, the ratio of the proportion of the rear secondary point number to the original secondary point number to the proportion of over-segmentation point number to the original over-segmentation point number is defined as the reduction rate of over-segmentation. The larger the ratio, the less pronounced the over-segmentation situation. The original number of secondary points is 394,605, while the original number of over-segmentation points is 4,460. The raw over-segmentation refers to the direct segmentation of the raw point cloud data without voxel filtering and secondary segmentation. This ratio can reflect the situation of over-segmentation under each voxel grid. It can be seen from Figure 8 that the effect of voxel filtering on the effective segmentation rate is relatively small, remaining around 93%. Only when the voxel grid is 0.10, there is a significant decrease. However, the over-segmentation gradually decreases with the increase of the voxel grid. The over-segmentation significantly decreases when the voxel grid is 0.09, at which point the effective segmentation rate also reaches a maximum value of 93.22%.

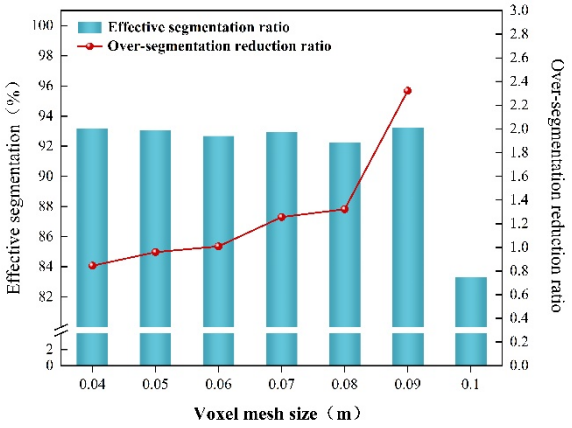

Figure 8
Effective segmentation and over-segmentation reduction under different voxel grids

The above experiments indicate that the optimal voxel grid edge length is 0.09 m, at which point the point intensity or average point spacing is 0.0643. The subsequent parameterization is based on a 0.09 m voxel grid.

Table 1
Segmentation under Different Voxel Grids

Size	Average point spacing	SL (Voxel filtering)	SL (Roughness filtering)	Initial segmentation	Over segmentation
0.04	0.0389	191,274	181,672	180,783	2,560
0.05	0.0432	145,614	137,982	137,180	1,715
0.06	0.0483	112,085	106,139	105,133	1,256
0.07	0.0533	87,487	82,763	82,092	787
0.08	0.0589	69,473	65,727	64,665	594
0.09	0.0643	56,303	53,345	52,763	220
0.10	0.0696	46,193	43,785	38,472	0

4.2 Rough Extraction

The work in this section is to remove the relatively rough parts in point cloud data. The roughly extracted point clouds retain most of the secondary point clouds, and this part of the point clouds is relatively dense without any missing points. However, the point cloud data at the initial support may be lost, due to the fact that the algorithm removes this part of the point clouds because of its large roughness.

There are two main factors that affect roughness screening: roughness calculation radius and roughness screening threshold. The roughness calculation radius represents the calculation radius of the neighboring point cloud fitting plane, and the roughness screening threshold is the distance from the points participating in the fitting plane to that plane. The parameters of the fitting plane are varied at different radii, and the distances from the neighboring point clouds to the plane also change accordingly. To determine these two parameters, algorithm experiments are conducted, where five different radii of 0.1, 0.15, 0.2, 0.25 and 0.3, are employed; and the optimal roughness radius and roughness screening threshold are determined by analyzing the optimal roughness threshold in each case.

Tables 2, 3 and 4 present the numbers of point clouds obtained by extracting and segmenting different roughness calculation radii with roughness extraction thresholds of 0.01, 0.02 and 0.03. The point cloud data utilized for roughness calculation are those previously obtained at the optimal point intensity, i.e., the point clouds filtered from the raw data at a voxel grid of 0.09. The total number of points is 606,195 and the number of secondary contrast points is 56,303. The ‘/’ in the table indicates that the secondary point clouds are not yet fully segmented or the over-segmentation is too severe.

Table 2

Number of extracted and segmented points with a roughness threshold of 0.01

Radius	Total number of points	Number of secondary lining points	Initial segmentation	Over-segmentation
0.10	380,620	48,718	48,062	562
0.15	345740	48,092	46,448	36
0.20	302,946	47,406	45,166	0
0.25	275425	46,766	44,888	0
0.30	256,713	46,012	44,008	0
0.35	240,533	44,928	42,451	0

Table 3

Number of extracted and segmented points with a roughness threshold of 0.02

Radius	Total number of points	Number of secondary lining points	Initial segmentation	Over-segmentation
0.10	462,185	53,886	/	/
0.15	472,637	53,830	54,238	844
0.20	429,963	53,359	53,032	274
0.25	396,835	52,893	52,487	169
0.30	374,259	52,465	51,923	0
0.35	352,963	51,955	51,396	0

Table 4

Number of extracted and segmented points with a roughness threshold of 0.03

Radius	Total number of points	Number of secondary lining points	Initial segmentation	Over-segmentation
0.10	490,930	54,613	/	/
0.15	535,788	54,865	/	/
0.20	504,899	54,505	55,251	1,027
0.25	475,140	54,128	54,152	581
0.30	453,471	53,777	53,766	519
0.35	432,602	53,450	53,429	498

Figure 9 presents the proportion of the extracted secondary point clouds to the overall point clouds for different calculation radii at roughness levels of 0.01, 0.02, and 0.03, while the original unextracted proportion was 9.29%. It can be seen that the overall trend of the proportion of the secondary point clouds increases with the increase of the calculation radius, while it decreases with the increase of the threshold value for the same calculation radius. Figure 10 presents the effective segmentation rates for a single segmentation at different computational radii with roughness values of 0.01, 0.02 and 0.03. The effective segmentation rates at roughness threshold of 0.01 are significantly lower than those of the 0.02 and 0.03, and there are more under-segmentation cases. However, at a roughness threshold of 0.03, there are more over-segmentation and ineffective segmentation cases. Therefore, the initial segmentation that can be used for subsequent secondary

segmentation should ensure that there are no over-segmentations and obvious gaps in space. From Figures 9 and 10, as well as Tables 2, 3 and 4, it can be inferred that the more suitable parameter combinations are 0.02-0.30 or 0.02-0.35, where the effective segmentation rate is higher for 0.02-0.30 than for 0.02-0.35. Therefore, the optimal parameter combination is 0.02-0.30.

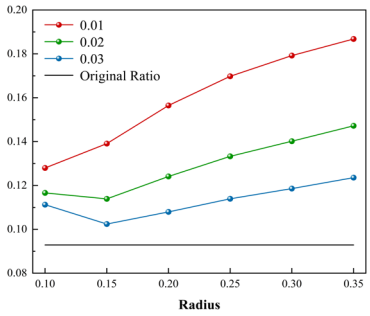

Figure 9

Proportion of extracted secondary point clouds to overall point clouds under different radii

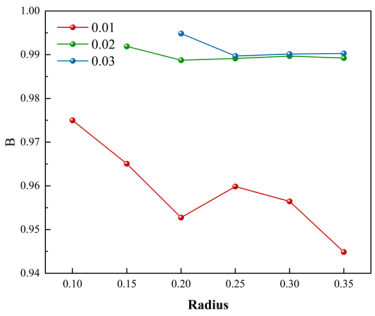

Figure 10

Effective segmentation rates for a single segmentation under different radii

4.3 Secondary Point Cloud Segmentation

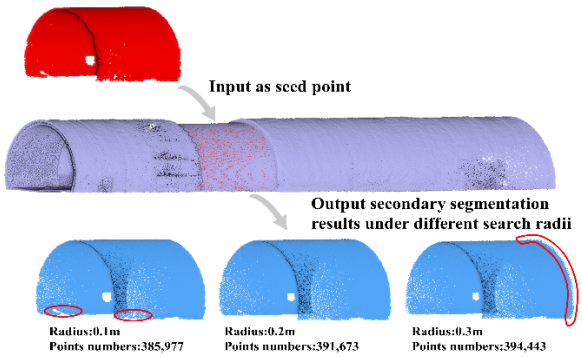

Figure 11

The segmentation results

The work in this section is to segment the secondary contrast point clouds in the point cloud data prior to voxelization. The optimal primary segmentation point clouds are determined by experimenting with the algorithm described above. The results of the primary segmentation are input into the raw data as seed points (i.e., the red point clouds in figure 11) for secondary segmentation. Three different calculation radii of the 0.1 m, 0.2 m and 0.3 m, are employed for secondary segmentation. The segmentation results are shown in the blue point clouds in figure 11, Some holes appear in the segmented point clouds at a radius of 0.1 m. The point clouds after segmentation at a radius of 0.3 m exhibit over-segmentation, with some

noise at the edges. These noise points are caused by the mobile scanning of the connection between the secondary lining and the initial support. The segmented point clouds with a calculation radius of 0.2 m have no obvious hole missing, and the impact of minimal noise can be ignored. It basically meets the requirements of the segmentation task, and the effective segmentation rate reaches 99.25%.

5 Discussion

5.1 Algorithm Evaluation and Comparison

To test the segmentation performance of the proposed algorithm for binary structures, four evaluation indicators of the accuracy, recall, F1 score, and union intersection [32] (IoU) are applied based on the true positive (TP), false positive (FP), true negative (TN), and false negative (FN). They are defined as follows:

$$\text{Precision}=\frac{\text{TP}}{\text{TP+FP}} \tag{4}$$

$$\text{Recall}=\frac{\text{P}}{\text{TP+FN}} \tag{5}$$

$$\text{F1-score}=\frac{2\times\text{Precision}\times\text{Recall}}{\text{Precision+Recall}} \tag{6}$$

$$\text{IoU}=\frac{\text{TP}}{\text{FP+TP+FN}} \tag{7}$$

Three algorithms are available for comparison: original roughness segmentation (no progressive aspect filtering, no secondary segmentation), surface curvature algorithm and DoN algorithm.

Surface curvature is a concept that describes the degree of variation of a point cloud surface based on the surface eigenvalues, which is different from the mathematical meaning of curvature. The Covariance matrix in Eq. (2) is decomposed into eigenvalues to obtain the eigenvalues of M. If $\lambda_0 \geq \lambda_1 \geq \lambda_2$ is satisfied, the surface curvature of point P is:

$$\sigma=\frac{\lambda_2}{\lambda_0+\lambda_1+\lambda_2} \tag{7}$$

where a smaller value of σ indicates a flatter and smoother neighborhood, while a larger value of σ indicates greater fluctuation in the neighborhood.

The DoN (Differential Operator Network) feature states that the surface normal vector estimated for a given radius can reflect the intrinsic geometric features of the surface. Therefore, this segmentation algorithm is based on normal estimation and requires the computation of the normal estimation of a point in the point clouds.

Selecting different support radii for a point in the point clouds can result in different estimations of the normal.

In this section the present algorithm is compared with three more widely used algorithms. The evaluation results of each algorithm are shown in Table 5, and the segmentation effectiveness of each algorithm is presented in Figure 12. It can be seen from Table 5 and Figure 12 that the original roughness algorithm and DoN algorithm suffer from severe over-segmentation problems, while the surface curvature algorithm undergo edge under-segmentation problems. The total number of the test point clouds is 14 million, and the total length of secondary lining is more than 120 m. The effect of long-distance segmentation is shown in Figure 13. In Figure 14, the quantity of point clouds processed per minute serves as the metric to assess or quantify the efficiency of the chosen algorithms.

Table 5
Evaluation Results of Each Algorithm

	TP	**FP**	**FN**	**TN**	**Precision**	**Recall**	**F1-score**	**IoU**
Ours	391,349	324	3,256	1,439,308	0.9925	0.9917	0.9954	0.9909
Original roughness	383,275	6,198	11,330	1,433,434	0.9841	0.9713	0.9776	0.9563
Surface variation	378,109	0	16,496	1,439,632	1	0.9582	0.9787	0.9582
DoN	316,082	4,673	78,523	1,434,959	0.9854	0.8010	0.8837	0.7916

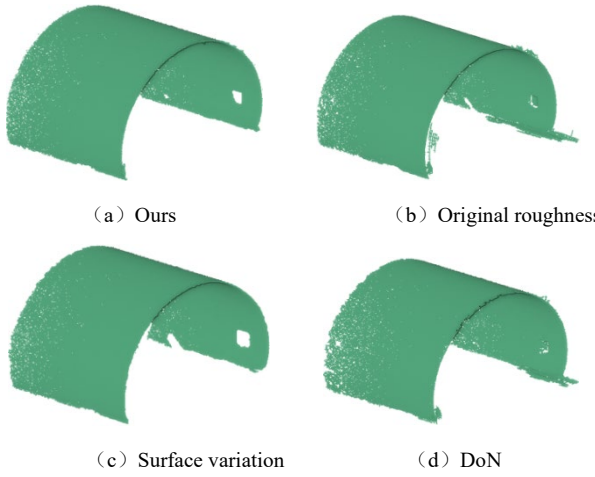

（a）Ours （b）Original roughness

（c）Surface variation （d）DoN

Figure 12
Segmentation Effect

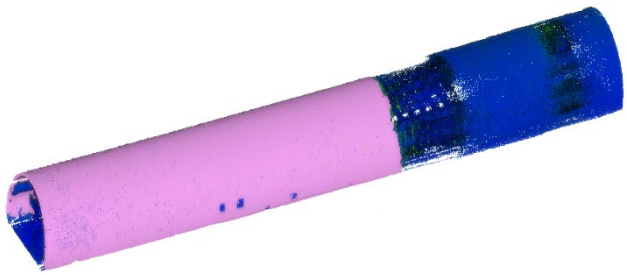

Figure 13
Long distance secondary lining segmentation effect

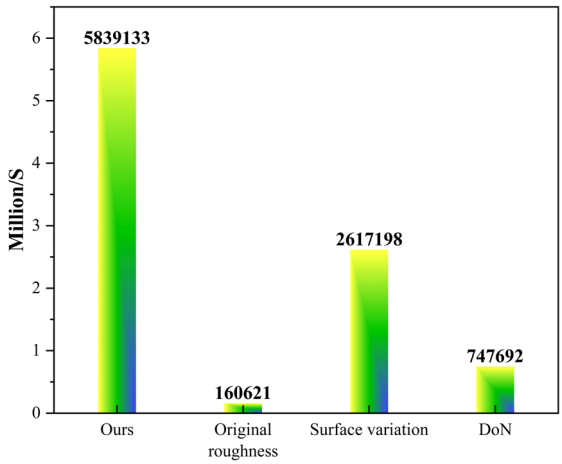

Figure 14
Comparison of Algorithmic efficiency

5.2 Engineering Applications

The method proposed in this paper can be used to segment the secondary lining point clouds without noise and allowing the number of points close to the raw data. Visualization and management of secondary lining progression and construction are of great importance in engineering. Therefore, the advancement information of the secondary lining is extracted.

The extraction of advancement information mainly includes: a) projecting the secondary point clouds towards the xoy plane; b) Extracting linear regions from projected point clouds; c) performing the polyline fitting for the extracted linear region; d) calculating the length of the obtained multiple branch lines and using the average value as the advancement distance. The extraction effectiveness and process are shown in Figure 15. The final extracted advancement distances are 12.18 m and 12.17 m, with an error of about 0.8% compared to the actual advancement distance. Therefore, the extracted advancement information is valid.

The extraction of advancement information mainly includes: a) projecting the secondary point clouds towards the xoy plane; b) Extracting linear regions from projected point clouds; c) performing the polyline fitting for the extracted linear region; d) calculating the length of the obtained multiple branch lines and using the average value as the advancement distance. The extraction effectiveness and process are shown in figure 15. The final extracted advancement distances are 12.18 m and 12.17 m, with an error of about 0.8% compared to the actual advancement distance. Therefore, the extracted advancement information is valid.

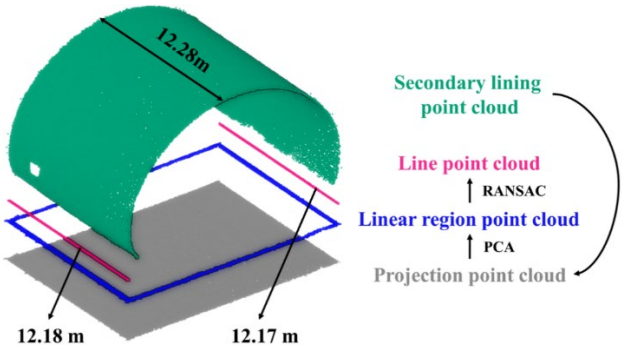

Figure 15
Extraction of advancement information

Conclusions

This paper proposes a roughness-based point cloud segmentation method. The optimal voxel parameters, roughness calculation radius and threshold are determined through algorithm experiments. The influence of parameters on the extraction and segmentation is analyzed. The primary segmentation is performed to primarily obtain the secondary lining point clouds; thereafter, the complete secondary lining point clouds are acquired through secondary segmentation. The algorithm effectiveness is evaluated and compared through the engineering application. The following conclusions are drawn:

(1) The analysis of the raw data indicates different differences in the normal vector components of the primary and secondary contrast point clouds on the three coordinate axes after laser radar scanning. The normal vectors of the secondary contrast point clouds vary uniformly while the normal vectors of the primary support and secondary lining point clouds vary abruptly. The analysis confirms that there are roughness differences between the secondary and primary contrast point clouds in the point cloud data.

(2) The key parameters including the optimal point intensity for segmentation, the calculation radius and threshold of the roughness extraction in the first segmentation, and the segmentation radius in the second segmentation are determined through algorithm experiments. The selected optimal parameters improve the algorithmic efficiency and segmentation accuracy.

(3) The proposed algorithm is evaluated and compared by using the accuracy, recall rate and F1 score as evaluation indicators. Compared with the original roughness and similar algorithms, the developed algorithm offers the best segmentation performance, with 99.25% accuracy and about 5.8-million-point clouds processed per minute.

References

[1] R. Hong, H. Huan, Development Trends and Reflections on Highway Tunnels in China in the Last 10 Years, China J. Highw. Transp., Vol. 33, No. 12, pp. 62-76, 2020

[2] A. Németh, S. K. Ibrahim, M. Movahedi Rad, S. Szalai. Laboratory and Numerical Investigation of Pre-Tensioned Reinforced Concrete Railway Sleepers Combined with Plastic Fiber Reinforcement. Polymers 2024, Vol. 16, No. 11, 2024, doi: 10.3390/polym16111498

[3] Q. Li, Research on tunnel construction quality based on visualization management, Applied Mechanics and Materials. Trans Tech Publications Ltd., Vol. 580, pp. 3192-3195, 2014

[4] W. Qu, Application of BIM Virtual Technology in Highway Tunnel Construction Management, Forthcoming Networks and Sustainability in the IoT Era: Second International Conference., Vol. 1, pp. 205-212, 2022

[5] Szabolcs Fischer. Evaluation of inner shear resistance of layers from mineral granular materials. Facta Universitatis, Series: Mechanical Engineering, DOI:10.22190/FUME230914041F

[6] L. Ren, Z. Wei, N. Liang, et al., Mechanical behavior of multi-scale fiber-reinforced concrete for secondary tunnel lining: Field test and numerical simulation, CASE STUD CONSTR MAT., Vol. 17, No. e01669, 2022

[7] Rabcewicz. L, Dhe New Austrian Tunneling Method, Part One. Water Power, pp. 453-457, 1964

[8] Rabcewicz. L, Dhe New Austrian Tunneling Method, Part Two. Water Power, pp. 511-515, 1964

[9] Rabcewicz. L, Dhe New Austrian Tunneling Method, Part Three Water Power, pp. 19-24, 1965

[10] L. Wan, L. Zhou, H. Sun, Development and Application of Steel Wood Composite End Formwork for Tunnel Secondary Lining Construction Joint, Mod Tunnel Technol., Vol. 56, No. 3, pp. 200-205, 2019

[11] László Ézsiás, Richárd Tompa, Szabolcs Fischer. Investigation of the Possible Correlations between Specific Characteristics of Crushed Stone Aggregates. Spectrum of Mechanical Engineering and Operational Research, Vol. 1, No. 1, pp. 10-26, 2024

[12] Lei Kou, Mykola Sysyn, Jianxing Liu, Influence of Crossing Wear on Rolling Contact Fatigue Damage of Frog Rail. Facta Universitatis, Series: Mechanical Engineering, https://doi.org/10.22190/FUME220106024K

[13] Q. Wang. M. Kim, Applications of 3D point cloud data in the construction industry: A fifteen-year review from 2004 to 2018. Adv. Eng. Inform., Vol. 39, pp. 306-319, 2019

[14] Y. Guo, H. Wang, Q. Hu, et al., Deep learning for 3d point clouds: A survey, IEEE T Pattern Anal., Vol. 43, No. 12, pp. 4338-4364, 2020

[15] W. Zhang, W. Qiu, D. Song, et al., Automatic tunnel steel arches extraction algorithm based on 3D LiDAR point cloud, Sensors., Vol. 19, No. 18, pp. 3972, 2019

[16] C. Fotsing, N. Menadjou, C. Bobda, Iterative closest point for accurate plane detection in unorganized point clouds, Autom. Constr., Vol. 125, 2021

[17] Y. Xu, Z. Ye, R. Huang, L. Hoegner, U. Stilla, Robust segmentation and localization of structural planes from photogrammetric point clouds in construction sites, Autom. Constr., Vol. 117, 2020

[18] X. Cheng, D. Jia, Y. Liu, et al., Tunnel point cloud denoising algorithm based on centerline, Journal of Tongji University, 2015

[19] L. Cui, L. Zhou, Q. Xie, et al., Direct generation of finite element mesh using 3D laser point cloud, Structures., Vol. 47, No. 1579-1594, 2023

[20] P. S. Dąbrowski, M. H. Zienkiewicz, 3D point‐cloud spatial expansion by total least‐squares line fitting, Photogramm Rec., Vol. 35, No. 172, pp. 509-527, 2020

[21] L. Yang, Y. Li, X. Li, et al., Efficient plane extraction using normal estimation and RANSAC from 3D point cloud, Comput. Stand. Inter., Vol. 82, No. 103608, 2022

[22] D. Duan, W. Qiu, Y. Cheng, et al., Reconstruction of shield tunnel lining using point cloud, Automat. Constr., Vol. 130, No. 103860, 2021

[23] B. Shi, M. Yang, J. Liu, et al., Rail transit shield tunnel deformation detection method based on cloth simulation filtering with point cloud cylindrical projection, Tunn. Undergr. Sp. Tech., Vol. 135, No. 105031, 2023

[24] X. Ma, W. Luo, M. Cheng, et al., A fast point cloud segmentation algorithm based on region growth. IEEE. Icocn., 2019

[25] X. Xie, Y. Wan, K. Yan, et al., 3D laser scanning point cloud region segmentation and volume calculation for underground caverns, J Electr Measur Instr., Vol. 33, No. 09, pp. 80-86, 2019

[26] A. Ji, Y. Zhou, L. Zhang, et al., Semi-supervised learning-based point cloud network for segmentation of 3D tunnel scenes, Automat. Constr., Vol. 146, No. 104668, 2023

[27] N. Ding, Y. Zhou, D. Li, K. Zeng, Real-time deformation monitoring of large diameter shield tunnel based on multi-sensor data fusion technique, Measurement, Vol. 225, No. 114061, 2024, DOI: 10.1016/j.measurement.2023.114061

[28] A. Ji, A. Chew, X. Xue, et al., An encoder-decoder deep learning method for multi-class object segmentation from 3D tunnel point clouds, Automat. Constr., Vol. 137, No. 104187, 2022

[29] J. Yu, J. Liao, Z. Chen, et al., A tunnel segment segmentation and section extraction based on point cloud model of cross-section datum plane, Bulletin of Surveying and Mapping., Vol. 10, No. 159, 2021

[30] G. Cao, X. Liu, N. Liu, Segmentation of subway tunnel wall surface objects based on laser 3D point cloud, Acta Optica Sinica., Vol. 40, No. 21, 2020

[31] C. Zong, H. Wang, An improved 3D point cloud instance segmentation method for overhead catenary height detection, Comput. Electr. Eng., Vol. 98, No. 107685, 2022

[32] H. Fu, Q. Song, J. Gong, L. Jiang, Z. Liu, Q. Luan, H. Wang, Automatic detection and pixel-level quantification of surface microcracks in ceramics grinding: An exploration with Mask R-CNN and TransUNet, Measurement, Vol. 224, No. 113895, 2024, DOI: 10.1016/j.measurement.2023.113895